

# The evolutionary stage of the semiregular variable QY Sge = IRAS 20056+1834

V.G. Klochkova, V.E. Panchuk, E.L. Chentsov, M.V. Yushkin

Special Astrophysical Observatory RAS, Nizhnij Arkhyz, 369167 Russia

November 1, 2018

**Abstract** Repeated spectral observations made with the 6-m telescope of SAO RAS yielded new data on the radial velocity variability of the peculiar yellow supergiant QY Sge. The strongest and most peculiar feature in its spectrum is the complex profile of NaI D lines, which contains a narrow and a very wide emissions. The wide emission can be seen to extend from  $-170$  to  $+120$  km/s, and at its central part it is cut by an absorption feature, which, in turn, is split into two subcomponents by a narrow (16 km/s at  $r=2.5$ ) emission. An analysis of all the  $V_r$  values leads us to adopt for the star a systemic velocity of  $V_r=-21.1$  km/s, which corresponds to the position of the narrow emission component of NaI. The locations of emission features of NaI D lines are invariable, which point to their formation in regions that are external to the supergiant's photosphere. Differential line shifts of about 10 km/s are revealed. Emission in the  $H\alpha$  line is weaker than in NaI D lines, it fills the photospheric absorption almost completely. The absorption lines in the spectrum of QY Sge have a substantial width of  $FWHM \approx 45$  km/s. The method of model atmospheres is used to determine the following parameters: the effective temperature  $T_{eff}=6250\pm 150$  K, surface gravity  $lg g=2.0\pm 0.2$ , and microturbulence velocity  $\xi_t=4.5\pm 0.5$  km/s. The chemical composition of the atmosphere differs only slightly from the solar composition: the metallicity of the star is found to be somewhat higher than the solar metallicity with an average overabundance of iron-peak elements of  $[Met/H]_{\odot}=+0.20$ . The star is found to be slightly overabundant in carbon and nitrogen,  $[C/Fe]=+0.25$ ,  $[N/Fe]=+0.27$ . The  $\alpha$ -process elements Mg, Si, and Ca are slightly overabundant, on the average by  $[\alpha/H]_{\odot}=+0.12$ , and sulfur overabundance is higher,  $[S/\alpha]=+0.29$ . The strong overabundance of sodium,  $[Na/Fe]=+0.75$ , is likely to be due to the dredge-up of the matter processed in the NeNa cycle. Heavy elements of the  $s$ -process are underabundant relative to the Sun. On the whole, the observed properties of QY Sge do not give grounds for including this star into the group of R CrB or RV Tau-type objects.

## 1. Introduction

The General Catalog of Variable Stars [1] classifies the yellow supergiant QY Sge (Sp=G0e) as a semiregular variable. The QY Sge star, associated with the IR source IRAS 20056+1834, is located outside the Galactic plane:  $b=-7^{\circ}.46$ .  $J$ - and  $H$ -band polarimetric observations [2] that were performed with UKIRT telescope revealed no extended structure or deviations from symmetry at the angular resolution of  $FWHM=0.67''$ . Polarization is constant throughout the entire image of the object, but decreases substantially with wavelength:  $P_J=14\%$ ,  $P_H=7\%$ . Gledhill et al. [2] classified IRAS 20056+1834 as a protoplanetary nebula (PPN) with a well-defined core (a "core-dominated object") and a compact optically thick envelope. We so far lack a conclusive answer to the question

about the physical mechanism of polarization in QY Sge in the absence of an extended envelope, however, submillimeter-wave observations with the 15-m James Clarke Maxwell Telescope (JCMT) also confirm the lack of such an envelope [3]. This led Gledhill et al. [3] to conclude that QY Sge is at the initial stage of the formation of its envelope. This conclusion is consistent with the high temperature ( $T_e \approx 600$  K) of the interstellar dust [4].

The attention that spectroscopists devote to the supergiant QY Sge is due to its complex optical spectrum, which includes photospheric and interstellar components, and, first and foremost, to the strong wide emission components of the D lines of NaI found even in the low-resolution spectra of the star [4]. Kameswara Rao et al. [5] were the first to study a high-resolution optical spectrum of QY Sge. The above authors identified the main spectral components (the absorption spectrum of the G-type supergiant combined with narrow low-excitation emission features and wide emission NaI D lines) and determined the chemical abundances of the atmosphere of the supergiant. They proposed a model of the system with a circumstellar torus and bipolar mass outflow. According to this model, the central star is completely obscured from the observer and we see the radiation reflected from the inner wall of the torus.

There is currently no consensus of opinion concerning the status of QY Sge (the proposed versions are: a massive supergiant, RV Tau or R CrB-type star, or a spectroscopic binary), its distance (the available estimates differ by one order of magnitude), and understanding of all the peculiarities of its optical spectrum. That is why we decided to spectroscopically monitor QY Sge with the 6-m telescope of the Special Astrophysical Observatory of the Russian Academy of Sciences (SAO RAS) and report the results of the first six years of observations in this paper.

## 2. Observations and data reduction

QY Sge is a rather faint object ( $V=12^m37$ ) for high resolution spectroscopy. We taken spectroscopic data with the PFES and NES CCD-echelle spectrographs of the 6 m telescope of SAO RAS. The spectrograph PFES [6] is mounted in the prime focus of the telescope and we used this spectrograph in 1998 to take the spectrum of QY Sge with a resolution of  $R=17000$  and a rather high signal-to-noise ratio ( $S/N \approx 100$ ). We used the NES spectrograph in 1998, 2002, 2003, and 2004 to take spectra with a resolution of  $R=60000$ , but with limited S/N ( $S/N \approx 40-50$ ). See [7, 8, 9, 10] for the description of the successive stages of the development and improvement of the NES spectrograph. The spectrograph NES uses an image slicer at its entry to cut the image into three slices to provide a more than double gain in flux [9]. Local corrector [11] ensures the accurate centering of the star's image relative to these slices. Wavelength calibration is performed using the central component of the echelle orders of the spectrum of the ThAr lamp and standard procedures of the ECHELLE context of MIDAS system for the reduction of CCD images.

The upper rows of Table 1 give the observing dates and operating wavelength region. The data obtained by Kameswara Rao et al. [5] complement fairly well the intensity and radial-velocity measurements of spectral lines given in the next rows of the table: the above authors took their spectra during the summer seasons of 1999, 2000, and 2001, which we missed, and have the same spectral resolution ( $R=60000$ ) as our observations.

We developed a dedicated code package [12] based on the ECHELLE context to modify the reduction of two-dimensional spectra taken with echelle spectrographs equipped with an image slicer. We extract each portion of a spectral order separately and then coadd the extracted components of the spectral order with the allowance for the wavelength shifts due to the design features of the image slicer. We determine the shift of each satellite slice of echelle orders along the dispersion of the echelle by cross-correlating with the emission spectrum of the hollow-cathode ThAr lamp also taken with an image slicer. Note that the shifts of the slices of the echelle orders along the

dispersion of the echelle allows more efficient removal of both cosmic-ray hits and CCD defects (“hot” pixels, “traps”, zero-sensitivity columns), because the same spectral features are located on different pixels of the detectors in the different components of spectral orders.

We use telluric lines to correct the dispersion curves. The residual systematic errors in radial velocities do not exceed 2 km/s for the spectra taken with PFES, and are lower than 1 km/s for other spectra. We estimated the measurement errors in pure form from the spectra taken with a one-day interval, on July 27 and 28, 2002. The radial velocities  $V_r$  measured at these observing times do not differ systematically and the mean errors range from 0.5 km/s for the strongest ( $0.4 < r < 0.55$ ) to 1.0 km/s for the weakest ( $0.85 < r < 0.8$ ) lines.

### 3. Peculiarities of the optical spectrum and radial velocities

Our observations confirmed the presence of main features earlier found in the optical spectrum of QY Sge: all our spectra show a very narrow,  $\Delta\lambda = 16$  km/s, and a wide,  $\Delta\lambda \approx 290$  km/s, emission components of NaI D lines. Metal absorptions are very wide: they are two-to-three times wider than the narrow NaI emission feature and this fact indicates that the latter formed in the circumstellar medium. We also point out the complex emission-and-absorption profile of H $\alpha$  (see Fig. 1). Note that none of our spectra shows the narrow emission lines with low-excitation metal lines identified by Kameswara Rao et al. [5].

#### 3.1. Identification and measurement of the parameters of spectral features

According to our estimates, which are close to those of [4] and [5], QY Sge has a spectrum of a late F-type supergiant with more than half of its lines belonging to iron. This fact allowed us to use the spectrum of the  $\alpha$  Per (Sp=F5 Ib) supergiant taken with the same instruments as the spectrum of QY Sge for identifying the lines and selecting the least blended among them and to adopt the laboratory wavelengths necessary for the determination of radial velocities mostly from the solar-spectrum tables [13].

Table 2 lists the identifications of the main lines that we used to study the radial-velocity pattern. The same table gives for all our spectra the central residual intensities “r” of the selected absorptions and the radial velocities inferred from the lower parts of their profiles. Figure 2 gives examples of dependencies  $V_r(r)$  between these two parameters. The scatter of data points on these relations allows one to judge about the real errors of the inferred  $V_r$ , which include not only measurement errors, but also uncertainties of the laboratory wavelengths, effects of unaccounted blending and local deformations of the dispersion curves employed. Variations of the scatter from one spectrum to another are due not only to different exposures, but also to the variations of the profile shapes with time. Figure 2 compares the  $V_r(r)$  dependencies obtained for the same spectral range from the spectra taken on August 16, 2003 (when the most symmetric and narrow metal absorptions were observed) and August 28, 2004. The mean errors of the determination of  $V_r$  estimated from these data based on a single line differ and are equal to 0.6 and 2.0 km/s, respectively. In view of the errors of the determination of  $V_r$ , we rounded the corresponding values in Tables 1 and 2 to 1 km/s.

Derivation of the mean velocities for individual dates requires the allowance for differential line shifts, which, according to our data, are real and variable: they are barely visible in the spectrum taken on August 16, 2003, but quite conspicuous in our other spectra. By their absolute magnitude (about 10 km/s) the maximum mutual shifts are close to those pointed out by Kameswara Rao et al. [5], but their behavior differs: instead of the sharp rebound of  $V_r$  as inferred from resonance lines and low-excitation absorptions, we observe monotonic increase of velocity with increasing line intensity (the lower  $V_r(r)$  curve in Fig. 2). However, such dependences can also be found by

analyzing the data given by Kameswara Rao et al. [5]. Two circumstances corroborate this: (1) the spectral resolution of [5] is at least as good as ours and their signal-to-noise ratio (judging from Figs. 1, and 2 adopted from [5]) is even higher than our S/N, whereas the errors of the mean  $V_r$  values reported by the above authors are close to our errors for a single line; (2) absorptions with low potentials of excitation of the lower level are among the strongest ones.

The slope of the  $V_r(r)$  relation can be affected by the line asymmetry, which is immediately apparent in the profiles of FeI lines shown in Fig. 3. In the spectra taken on August 28, 2004 the absorption cores are redshifted relative to the wings, and are more conspicuous compared to the profiles of deeper lines. As a result, the velocity measured at half the central depth (the mean velocity for the line as a whole) increases with depth to a lesser extent than the velocity measured from the bottommost part of the profile (the crosses and squares in Fig. 2, respectively).

The two rows of Table 1 give the  $r$  and  $V_r$  values (corresponding to the lower parts of the profiles of photospheric absorptions) for the right-hand ends of the  $V_r(r)$  curves represented by the lines of the 15th FeI multiplet. Below, rows 4 and 5 of the same table give the same quantities for the weakest lines (the left-hand ends of the  $V_r(r)$  curves). The table confirms the conclusion about the radial-velocity variability of QY Sge made by Kameswara Rao et al. [5]. Unfortunately, the above authors did not analyze differential line shifts in the spectra of QY Sge and give only the mean velocities (from  $-23$  to  $-9$  km/s) averaged for each season, which, however, agree well with our velocities. To illustrate the variable asymmetry of the FeI (15) line, we give in row 3 of Table 1 the shifts of the data points on the blue and red slopes of the line profiles relative to the line cores, measured at half of their depth. To reduce noise, we averaged the profiles of several absorptions of similar intensity and show the result in Fig. 3. As is evident from the figure, the profiles obtained in 2003 and 2004 are not just asymmetric, but appreciably deformed. On both the red slope of the former profile and the blue slope of the latter profile averaging confidently reveals depressions similar to those observed in the spectra of SB2 binaries. However, these results do not confirm the hypothesis about the binary nature of the star: it assumes that both the primary and secondary components of the profile should shift in opposite directions. However, the 2003 profile is redshifted entirely relative to the 2004 profile. A comparison of the spectra taken in 2002 and 2003 also shows that variations of microturbulent velocity and/or radial gradient of velocity in the star's atmosphere can be neither the only nor even the main cause of the variations of absorption profiles. The increase of the line depth in the first spectrum is not accompanied by their broadening and intensification. This is especially apparent in absorptions of moderate and low intensity ( $r \geq 0.7$ ). Both the specific shape of the profiles and the nature of its variations can be explained by the scattering of the star's radiation by the dust envelope with inhomogeneous density distribution. Scattering on dust grains is known to cause the broadening and asymmetry of photospheric absorptions and their shift toward longer wavelengths [14]. Such a redshift has been known since long, but it could be confidently detected only after the measurement of the systemic velocities of cool supergiants from the hydroxyl lines in their spectra (see, e.g., [15]). The blue POSS-2 plate image (<http://archive.stsci.edu/dss>) of the area surrounding QY Sge shows a scattering dust nebular (with a size of up to  $30''$ ), which suggests the presence of an expanding dust shell near the star.

### 3.2. Peculiar profile of the NaI D lines

The emission lines (or components) of the sodium doublet can be seen in the spectra of a number of well-studied post-AGB stars. For example, the spectrum of the high-latitude supergiant 89 Her contains a weak emission feature, which is blended with what appears to be an interstellar absorption [16]. A complex emission-and-absorption profile of NaI D lines can also be seen in the very high-resolution ( $\approx 10^5$ ) spectrum of HR 4049 taken by Bakker et al. [17] with the CES spectro-

graph attached to CAT telescope. Bakker et al. [17] suggested that the variability of part of the NaI components is due to variable emission.

We use NaI D lines to analyze the structure of the circumstellar matter in the QY Sge system. The local corrector of the star’s position can be tuned so as to make the portions of the image located at different distances from the center of the star’s image to be projected onto different sections of the image slicer (each with a size of  $0.6 \times 1.8$  arcsec). In the case of about 1 arcsec seeing and image-corrector errors no greater than 0.1 arcsec it is safe to say that the fractions the flux coming from the star and its neighborhood differ for different sections. Fig. 4 shows the profiles of NaI D lines for three angular distances from the star’s center. We point out three important features of this figure. First, the relative intensities of narrow emission features remain unchanged after the normalization of each of the spectra to its own continuum level. The most simple explanation of this phenomenon consists in the assumption that the size of the formation region of the narrow lines of the sodium doublet is smaller than the angular resolution of the telescope. Second, the intensity ratio of the lines of the doublet is close to unity, whereas in the absence of self absorption the upper levels are populated proportionally to their statistical weights and the ratio in question must be close to two. Equal intensities can be explained either by the high concentration of sodium atoms when resonance scattering on lines levels out the intensity ratio of the emission components (in this case the number of atoms along the line of sight must be no less than  $10^{10} \text{ cm}^{-2}$ ), or by the mechanism of resonance fluorescence, where the ratio of emission intensities is determined by the ratio of the illuminating fluxes (in the cores of the lines of the photospheric spectrum). Fluorescence can be observed only in the case where the illuminating source (the star) cannot be directly observed and its radiation does not exceed the weak fluorescence. Third, it is evident from the wide (high-velocity) components of the lines of the doublet that the contribution of blueshifted emission increases and that of redshifted emission decreases with increasing distance. The enhancement of the blueshifted emission as we move from the star along the nebula indicates that we observe the ever increasing relative contribution from the regions of the circumstellar shell that move toward us, whereas the contribution of receding regions remains virtually unchanged. This effect can be explained assuming that the regions where the line-of-sight velocity of gas is directed “toward” and “away from” observer are spatially separated (within a 1.8 arcsec square). If we further assume that high-velocity motions are axisymmetric (as Kameswara Rao et al. [5] adopt in their model), the data shown in Fig. 4 can be used to estimate the ratio of the opening angle ( $\alpha$ ) of the cones in which the high-velocity motions are contained and the tilt angle ( $\beta$ ) of the cone axis to the sky plane:  $\beta + \alpha/2 = 90^\circ$ . And, finally, Fig. 4 leads us to conclude that profiles of such a shape can be observed only in the cases where the radiation of the central star is strongly absorbed, i.e., if the star is partially or totally hidden from direct observation. For example, R CrB-type stars (UW Cen [18], S Aps [19] and R CrB itself [20]), and FG Sge [21] exhibit similar profiles of the resonance sodium doublet during periods of light decline with the only exception that their high-velocity components are much wider and overlap, and narrow emissions are also rather wide (about  $0.5 \text{ \AA}$ ).

Let us consider the temporal variations of NaI D lines. Table 1 lists the parameters of the emission-and-absorption profile of the resonance NaI D2 line in the spectrum of QY Sge at all our observing times and Fig. 5 shows its shape and temporal variations. The  $r$  values in Table 1 correspond to the peaks of the narrow emission feature and to the highest of the two wide emission humps, and to the core of the deepest (redshifted) absorption component, whereas the  $V_r$  quantities correspond to the upper part of the emission peak and lower parts of the wide emission and absorption as a whole. The profile agrees with that described by Kameswara Rao et al. [5] to the last detail. It consists of a wide emission, which can be seen to extend from  $-170$  to  $+120 \text{ km/s}$  and whose central part is cut by an absorption feature, which, in turn, is parted in two by a narrow

(16 km/s at  $r = 2.5$ ) emission peak. The narrow emission and the base of the wide emission are symmetric. The absorption is asymmetric: it is abruptly bound on the red side (the entire intensity drop fits inside the  $0 < V_r < 15$  km/s interval), and the lower part of the blue wing is also abrupt, but it has a bend at  $V_r \approx -50$  km/s, the wing becomes flat and extends at least out to  $V_r \approx -95$  km/s.

We use the  $V_r$  values for the absorption as zero points for estimating the extent of its blue wing. We give these estimates ( $\Delta V_r$ ) in the same Table 1. It is evident from Fig. 3 in the paper by Kameswara Rao et al. [5] that the long-wavelength component of the high-velocity profile becomes stronger in the spectrum taken in 2000 compared to the spectrum taken in 1999. Our subsequent observations (Fig. 5) confirm this variability of the spectral profile ignored by the above authors. On the whole, it is safe to say that we have found conclusive evidence for the temporal variability of the intensity of the narrow emission and the ratio of the intensities of the humps of the wide emission, although the positions of the main components of the profile remain unchanged on the radial-velocity scale.

The fixed position of the NaI emission features implies that they form in the regions that are external to the photosphere of the supergiant. The main problem for interpreting the NaI (1) profile is the narrow emission that overlaps the absorption core. With this feature ignored, the profile can be represented as a combination of the P Cyg-type wind profile and interstellar absorption. Photospheric absorption must also be present, however, it cannot contribute significantly: it could only slightly lower the central part of the wide emission – by no means to the continuum level – and, as is evident from Table 1, the absorption component of the NaI line reproduces neither the radial velocities of strong FeI photospheric lines nor their oscillations. As for the P Cyg-type profile, here we mean its type III variant according to Beals [22]: blueshifted absorption between two emission humps with the blue hump significantly higher than the red hump. In our case the latter condition is not satisfied, because the red component is trimmed and weakened by interstellar absorption. According to the available data ([23] et al.), the mean heliocentric radial velocity of the interstellar medium in the solar neighborhood at the Galactic latitude of QY Sge ( $l = 58^\circ$ ) is equal to about  $-15$  km/s and lies in the  $0 \div 10$  km/s interval at greater distances. The red component of absorptions, which is deeper in the NaI (1) profile and dominates in the profile of the KI (1) 7699Å resonance line, falls just within this velocity interval.

### 3.3. The $H\alpha$ profile

Compared to NaI (1) lines, the  $H\alpha$  line in the spectrum of QY Sge is less pronounced, but the resemblance of their profiles is evident. Unfortunately, Kameswara Rao et al. [5] do not report their  $H\alpha$  profile, but only point out that the  $H\alpha$  is comparable to the broad NaI (1) emission feature. Our data too corroborate this result, as is evident from Fig. 1, which shows the profiles of both lines in the spectrum taken in 2004 along with the  $H\alpha$  profile in the spectrum of the comparison star  $\alpha$  Per *F5Ib*.  $H\alpha$  is weaker than emission in NaI(1) lines, it almost floods the photospheric absorption, resulting in a small intensity difference:  $0.7 < r < 1.1$ . This line is totally indistinguishable in the low-resolution spectra taken by Menzies and Whitelock [4]. Photospheric wings, especially the short-wavelength one, are clearly visible, however, we bear in mind the problems associated with drawing the continuum of the echelle spectrum and restrict our analysis to investigating the central, wind-produced, part of the spectrum. The spectrum of QY Sge does not show the narrow emission in  $H\alpha$  (see Fig. 1, it was also removed from the NaI profile), and the positions and relative heights of broad emission humps repeat themselves in the profiles of the  $H\alpha$  and NaI features. The same appears to be true for the positions of the absorptions that separate the peaks, and small discrepancies between the  $V_r$  values listed in Table 1 may be due to the interstellar component of the NaI feature.

It is also possible that the wind-produced absorption in H $\alpha$  also contributes (along with the TiII 6560 Å line) to the depression at  $V_r \approx -150 \div -200$  km/s.

#### 4. Determination of model parameters and chemical abundances

Absorption lines in the spectrum of QY Sge have a substantial width,  $FWHM \approx 45$  km/s. Such a broadening of the profiles of photospheric absorption lines is observed in the spectra of a number of post-AGB stars. For example, the widths of photospheric lines in the spectrum of AFGL 2688 may be as high as 40 km/s [24, 25]. The mechanisms of such a strong line broadening in the spectra of supergiant stars are not yet entirely understood. Attempts have been made to explain the broadening in the spectrum of AFGL 2688 by scattering on moving dust [25], when we see only the radiation scattered by dust and the star is hidden by a dust torus.

Most of the lines in the spectrum of QY Sge are strongly blended because of their appreciable width, thereby complicating the measurement of their equivalent widths. We measured most of the equivalent widths  $W_\lambda$  of the lines in the highest signal-to-noise ratio spectrum taken with PFES; in some cases we measured  $W_\lambda$  in higher-resolution spectra taken with the NES spectrograph. The increased spectral resolution gives no advantages for identifying spectral features, but allows more accurate separation of blends. In addition, high spectral resolution allows complex profiles with narrow emissions to be resolved into individual components.

We apply the method of model atmospheres to numerous iron lines to determine the parameters of the star's atmosphere. As a first approximation, we use the atmospheric parameters of QY Sge obtained by Kameswara Rao et al. [5]. We determine the effective temperature  $T_{eff}$  from the condition that the iron abundance determined from individual FeI lines should be independent of the excitation potential of the corresponding lines. We fix surface gravity  $\log g$  based on the condition of ionization balance, i.e., that the iron abundance determined from FeI lines must be equal to the iron abundance determined from the lines of FeII. We determine the microturbulence velocity  $\xi_t$  from the condition that the iron abundance must be independent of the equivalent width of the corresponding FeI lines. In our computations we use Kurucz's [26] grid of models and WIDTH9 program to determine the elemental abundances. We adopt the excitation potentials and oscillator strengths for all lines, as well as broadening constants from VALD atomic line database [27].

Like in the case of most of the supergiants, we could not find a single microturbulence velocity to fit the full set of lines forming at different depth in the atmosphere of QY Sge. Figure 6a shows the iron abundance  $\log \epsilon(\text{Fe})$  as a function of the equivalent width of individual FeI lines (circles) at  $\xi_t = 4.5$  km/s. As is evident from the figure, with the adopted parameters of the model atmosphere the iron abundances determined from weak lines with equivalent widths  $W_\lambda < 240$  mÅ (filled circles) are independent of the line intensity. The dashed line shows the regression relation based on weak lines. At the same time, strong lines with  $W_\lambda > 240$  mÅ (open circles) deviate significantly toward higher  $\log \epsilon(\text{Fe})$ . The attempts to determine the microturbulence velocity from strong lines yield  $\xi_t = 15$  km/s. This situation is often explained by the variation of the microturbulence velocity with depth in the star's atmosphere. Deviations from local thermodynamic equilibrium (LTE) in the atmospheres of supergiant stars also play an important part: strong lines are usually more sensitive to non-LTE effects. The allowance for deviations from LTE for FeI lines makes the variation of microturbulence velocity with depth somewhat more pronounced [28] and therefore the increase of  $\xi_t$  for stronger lines cannot be explained by deviations from LTE in the atmosphere of QY Sge. This conclusion is indirectly corroborated by a similar result obtained from FeII lines, although the latter are less sensitive to non-LTE effects. The triangles in Fig. 6 show the results obtained for FeII lines: the filled and open triangles correspond to the lines with  $W_\lambda < 240$  mÅ and  $W_\lambda > 240$  mÅ,

respectively. The microturbulence velocity  $\xi_t=4.5\pm 0.5$  km/s that we determined from weak lines agrees with the results obtained by Kameswara Rao et al. [5].

Figure 6b shows the iron abundance,  $\log \epsilon(\text{Fe})$ , as a function of the excitation potential  $\chi_L$  of the lower level of the corresponding transition. The dashed line shows the result of linear regression for FeI lines with  $W_\lambda < 240$  mÅ (filled circles). At  $T_{eff} = 6250 \pm 150$  K the iron abundance inferred from weak FeI lines does not correlate significantly with excitation potential. Our excitation temperature is somewhat higher than the temperature  $T_{eff}=5850 \pm 200$  K determined by Kameswara Rao et al. [5], however, the discrepancy is insignificant given the errors of temperature determination.

The iron abundances determined from FeI and FeII lines agree within the measurement errors at the surface gravity value of  $\log g = 2.0 \pm 0.2$ . For the given parameters of the atmosphere of QY Sge the group of 66 weak FeI lines yields an average iron abundance of  $\log \epsilon(\text{Fe})=7.64$ , which is 0.14 dex higher than the solar value. The group of eight weak FeII lines yield the same iron abundance,  $\log \epsilon(\text{Fe})=7.64$ . It is evident from Fig. 6a that for parameters  $T_{eff} = 6250$  K,  $\log g = 2.0$ , and  $\xi_t = 4.5$  km/s of the model atmosphere of QY Sge the iron abundances determined from FeI and FeII lines agree throughout the entire range of equivalent widths. Our result for the surface gravity,  $\log g=2.0$ , differs significantly from the  $\log g=0.7$  obtained by Kameswara Rao et al. [5], and this fact appears to indicate that the luminosity of the star is lower than it has been so far believed.

Figure 7 compares the observed spectrum of QY Sge in the neighborhood of the  $H_\beta$  line and the theoretical spectrum computed with our atmospheric parameters using *SynthV* program [29]. The good agreement between the two spectra, first, shows that we have correctly chosen the fundamental parameters of the atmosphere of QY Sge, and, second, disproves the hypothesis that QY Sge might belong to the class of R CrB-type variables characterized by the underabundance of hydrogen in their atmospheres.

The list of lines with measured equivalent widths and elemental abundances computed from individual lines is available at <http://ales.sao.ru/ftp/pub/QYSge-lines.html>. When computing the chemical composition of the star we use, like in the case of the determination of its atmospheric parameters, spectral lines with equivalent widths  $W_\lambda < 240$  mÅ. Table 3 lists the computed abundances for various chemical elements in the atmosphere of QY Sge averaged over the entire set of the lines employed. The same table also gives the standard deviations  $\sigma$  of elemental abundances and the number of lines, “n”, used in the analysis. The dispersion serves as a good indicator of the accuracy of observational data for elements with sufficiently large number of lines. As is evident from the table, the standard deviation usually does not exceed  $\sigma < 0.27$  dex in the cases where the number of lines  $n > 8 \div 10$ . The factors that contribute to the errors of observational data include, besides the errors of observational data, the uncertainty of the parameters of the adopted model atmosphere. Table 4 lists the errors due to the uncertainty of the main parameters of the star. As is evident from the table, the large abundance errors arise from the uncertainty of the inferred effective temperature, especially for the lines of neutral atoms with low excitation potentials. In the case of ion lines the uncertainty of surface gravity,  $\log g$ , is the dominating source of error. The uncertainty of microturbulence velocity contributes only slightly to the abundance error, because we use sufficiently weak lines with  $W_\lambda < 240$  mÅ. One must bear in mind the following two circumstances: first, parameters of the model atmosphere are not mutually independent (e.g., a change in temperature entails a change in surface gravity), and, second, the determination of relative abundances (with respect to iron) reduces the error due to the uncertainty of the parameters of the model atmosphere.



## 5. Discussion of results

### 5.1. Elemental abundances

As we pointed out above, the iron abundance in the atmosphere of QY Sge,  $[Fe/H]_{\odot}=+0.14$ , is somewhat higher than the solar iron abundance. The overabundance of iron-peak elements is even higher and reaches its maximum for manganese,  $[Mn/H]_{\odot}=+0.35$ , whereas the zinc abundance is almost at the solar level,  $[Zn/H]_{\odot}=+0.04$ . The average overabundance of the iron-peak elements V, Cr, Mn, Fe, Co, Ni, Cu, and Zn is equal to  $[Met/H]_{\odot}=+0.20$ . The good agreement between the V and Cr abundances determined from the lines of neutral atoms and ions confirms the correctness of our determination of surface gravity.

We calculate the abundances of two elements – carbon and nitrogen – of the CNO group. We determine the nitrogen abundance from the easily identifiable  $\lambda 7468 \text{ \AA}$  line, whereas the other neutral nitrogen lines available in the recorded wavelength region are blended. We find carbon and nitrogen to be overabundant and the C/N ratio in the atmosphere of QY Sge to be close to its solar value. Such a C/N ratio is indicative of dredge-up. The carbon abundance decreases as a result of the dredge-up of the matter processed in the CNO cycle as convection develops after the star leaves the main sequence. At the same time, nitrogen abundance increases and therefore the C/N decreases. During subsequent evolution of the star the carbon abundance increases and nitrogen is processed into heavier elements via nuclear synthesis reactions involving  $\alpha$  particles. The C/N ratio again increases during the dredge-up of the matter that participated in helium burning reactions. It is possible that in the case of QY Sge we observe in the star’s atmosphere the matter processed both during hydrogen burning in CNO and NeNa cycles and during the  $\alpha$ -process.

The abundances of elements of the group of light metals are also, on the average, higher than the corresponding solar abundances. The  $\alpha$ -process elements Mg, Si, and Ca are only slightly overabundant: on the average,  $[\alpha/H]_{\odot}=+0.12$ , whereas sulfur is somewhat more overabundant,  $[S/\alpha]=+0.29$ . The scandium abundance is equal to its solar value within the measurement errors. Titanium, on the other hand, is underabundant, and its abundance determined from TiII lines is much lower than the solar value. TiI lines in the spectrum of QY Sge are very weak and measurement errors are comparable to the equivalent widths. We hence consider the result obtained from TiII, namely  $[Ti/H]_{\odot}=-0.42$ , to be more reliable.

Among the light metals sodium is most overabundant:  $[Na/H]_{\odot}=+0.89$ . The sodium overabundance is often explained by the high sensitivity of the lines of this element to non-LTE effects. In the spectra of supergiants NaI lines are usually strongly enhanced compared to the LTE case and therefore non-LTE corrections to the sodium abundance determined from individual lines may reach  $-0.75$  for supergiant stars [31]. We compute the Na abundance in the atmosphere of QY Sge using the weak subordinate lines 5682, 5688, and 6160  $\text{\AA}$ , which are less sensitive to non-LTE effects. If computed with the non-LTE corrections adopted from [31] for the parameters of the atmosphere of QY Sge, the sodium abundance is equal to  $[Na/H]_{\odot}=+0.83$ , which agrees with the abundance determined in terms of LTE approximation within the quoted errors. Hence the sodium overabundance of  $[Na/Fe]=+0.75$  observed in the atmosphere of QY Sge is mostly due to the dredge-up of the matter processed during the NeNa cycle of hydrogen burning.

The abundances of *s*- and *r*-process heavy elements do not allow unambiguous interpretation. The *s*-process element Ba is overabundant relative to iron,  $[Ba/Fe]=+0.33$ , whereas another *s*-process element, Nd, is slightly underabundant,  $[Nd/Fe] = -0.18$ . One must bear in mind that BaII lines are very strong in the spectrum of QY Sge and even the weakest of these lines located at 5853  $\text{\AA}$  – we use its intensity to determine the barium abundance – has the equivalent width of  $W_{5853}=260 \text{ m\AA}$ . Other, even stronger, lines yield even higher barium overabundance. The *r*-process element Eu is also slightly overabundant,  $[Eu/Fe]=+0.26$ . Yttrium forms in the course of both *s*-

and  $r$ -processes, however, this element is substantially underabundant in the atmosphere of QY Sge,  $[Y/Fe]=-0.82$ .

It is interesting that the atmosphere of QY Sge exhibits strong underabundance of two elements – Y and Ti – characterized by the highest condensation temperature,  $T_{cond} \approx 1600$  K. We could follow Kameswara Rao et al. [5] and assume that in the case of the star considered we observe only the effects of condensation of refractory elements. Such effects are often observed in RV Tau-type stars. However, this hypothesis is inconsistent, first, with the close to solar zinc-to-scandium abundance ratio,  $[Zn/Sc]=+0.05$ , whereas the  $T_{cond}$  values for these two elements differ by almost one thousand degrees. The same is also true for the zinc–calcium pair,  $[Zn/Ca]=-0.03$ , with equally large difference of  $T_{cond}$ . Second, the high iron abundance is also indicative of the low efficiency of condensation process in QY Sge.

## 5.2. The radial velocity pattern

The pattern of radial velocities  $V_r$  in the spectra of RV Tau-type stars is rather complex: it includes orbital motion with periods ranging from several months to several years along with other types of motions. For example, the orbital period of AC Her – a typical and well-studied RV Tau-type star –  $P_{orb} \approx 1200^d$  [32] is complemented by the pulsation component with a characteristic period of  $P_{puls} \geq 20^d$ , and also by the likely precession of the circumstellar disk (torus). It is evident that long-term homogeneous spectroscopic monitoring needs to be performed on the time scales of all the instability types mentioned above.

Our radial-velocity measurements based on the absorption spectrum of QY Sge confirm and extend the conclusion of Kameswara Rao et al. [5] about the variations of  $V_r$  both with time and from one line to another. The available observational data are still insufficient for directly testing the hypothesis that QY Sge is an RV Tau-type object and/or a binary. At the same time, we gathered new evidence in favor of the model suggested by Menzies and Whitelock [4] and elaborated by Kameswara Rao et al. [5]. According to this model, a substantial part of the star’s radiation accessible for us (if not the entire radiation) originates from the inner parts of a toroidal dust shell. The kinematic situation in the visible part of the torus determines the width and shift of the line as a whole, whereas the hypothesis of inhomogeneous dust density distribution is to be invoked to explain the discrete components of the “ragged” profile of the line (see Fig. 3).

Although the IR colors of the object are similar to those observed in OH/IR stars, the radio spectrum of QY Sge lacks the spectral features inherent to these objects [34, 33], which would allow us to determine the systemic velocity. To a first approximation, the systemic velocity can be determined from the available data by the position of the narrow emission component of NaI. We can assume that it forms in the peripheric regions of the envelope with low velocity gradients and is therefore symmetric, free of wind-induced deformations, and stationary. However, in this case two effects are difficult to explain: the variation of the intensity of the narrow emission component over a one-year time scale (Fig. 5) and the decrease of this intensity with the distance from the center of the star’s image proportionally to the decrease of continuum flux (Fig. 4). Within the accuracy of measurements the velocity inferred from this narrow emission is equal to  $V_r=-21.1$  km/s. We adopt this value as our first approximation to systemic velocity  $V_{sys}$ . The conclusion that the wide NaI emission is radiated by an extended envelope that spans far beyond the torus follows both from the lower polarization in this emission compared to the neighboring continuum [42] and the constancy of the radial velocity determined from the base of the profile. The mean velocity  $V_r=-32.4$  km/s of the broad emission is also stable within the measurement errors. The assumption that both Na D emission features form in the circumstellar envelope leads us to conclude that the envelope is nonuniform.

The model of Kameswara Rao et al. [5] leaves a number of questions unanswered that concern, first, the existence of emission features whose widths differ by one order of magnitude and, second, the mutual shift of the broad and narrow emission components of Na D.

Note that the model of the QY Sge proposed by Kameswara Rao et al. [5] is not the only one possible. The peculiarities of the observed optical spectrum mentioned above can also be explained in terms of a model of a binary system without a torus. A similar set of spectral features may form in the extended and inhomogeneous atmosphere of a supergiant star outflowing via stellar wind. Adopting the model of an optically thick torus makes it impossible to estimate the distance to QY Sge via standard spectral-and-photometric method, however, it allows us to avoid the difficulties associated with this method. We may limit the heliocentric distance to only several hundred parsecs [5] instead of the 9–36 kpc, inferred using the method just described by Menzies and Whitelock [4].

### 5.3. Whether QY Sge is an RV Tau-type star

Kameswara Rao et al. [5] are inclined to believe, based on the inferred parameters  $T_{eff}$  and  $\log g$  and the detailed analysis of its chemical composition, that QY Sge is an RV Tau-type star. Maas et al. [35], who analyzed the chemical composition of a sample of pulsating RV Tau-type stars, later used the results of Kameswara Rao et al. [5] within the framework of the same criterion. The chemical composition of QY Sge determined from the data obtained by Kameswara Rao et al. [5] indeed resembles the elemental abundances in the atmospheres of pulsating long-period variables. Such objects are usually only slightly metal underabundant. Given that the underabundance of metals is partially due to selective condensation of metal nuclei onto dust grains, the metallicity of RV Tau-type stars can be considered to be close to the metallicity of stars of the Galactic disk. It follows from the compilation in Table 9 from [35], that for classic RV Tau-type stars the initial (i.e., corrected for the effect of condensation) metallicity is equal, on the average, to  $[Fe/H]_{\odot} \approx -0.5$ . The mean “corrected” metallicity,  $[Fe/H]_{\odot} \approx -0.2$ , determined by Maas et al. [35] for a sample of stars with IR excess (including QY Sge) which in the diagram of IR colors are located in the domain of RV Tau-type stars, is even closer to the solar value.

However, the chemical composition similar to that observed in RV Tau-type stars is not unique. The same pattern of elemental abundances – weak metal underabundance, nonstandard abundances of CNO and  $\alpha$ -process elements, underabundance (in extremely rare cases, overabundance) of heavy metals – can be found among the post-AGB supergiants studied, which do not belong to RV Tau-type stars. Examples include the post-AGB stars HD 161796 and HD 331319 [36] or HD 133656 [37]. RV Tau-type stars display a wide variety of chemical-composition peculiarities, because they are determined both by the subtype of the Galactic population they belong to and by the initial mass and subsequent evolution of each particular star. Earlier, Wallerstein [38] also pointed out that metallicity (and chemical-composition peculiarities as a whole) of RV Tau-type stars is not the fundamental parameter that would allow a particular star to be attributed to this type. Hence the metallicity parameter or chemical composition as a whole do not allow us to classify QY Sge as an RV Tau-type star.

Shocks are known to propagate in the atmospheres of pulsating stars and the main indicators of these shocks are the blueshifted emission in hydrogen lines and asymmetric (or split) metal absorptions [39]. This can be illustrated by the spectrum of ACHer. However, the spectrum of QY Sge does not exhibit such features even if taken with a resolution of  $R = 60000$ , and this fact too casts doubt on the hypothesis that QY Sge may be an RV Tau-type star. The fact that the spectra of RV Tau-type stars lack wide Na I and K I D-line emissions provides yet another piece of evidence that is inconsistent with QY Sge being an RV Tau-type star.

#### 5.4. Whether QY Sge is an R CrB-type star

Wide emission components of the lines of the sodium doublet allows us to consider the possibility of including QY Sge into the so far small group of stars with such a spectral peculiarity (R CrB-type and selected post-AGB-type stars). A good example is provided by UW Cen, which is an R CrB-type star whose spectrum at minimum light shows a NaI D line profile with both a broad and narrow emission components [18]. The broad NaI emission in the spectrum of UW Cen [18], like in the spectrum of QY Sge, is blueshifted relative to the narrow component. There are other examples as well: S Aps [19], V854 Cen [40], and Z UMi [41]. It is important that both these components show up only when the star is at minimum light and are absent at maximum light. Note that emissions in the spectrum of QY Sge have been observed at all observational epochs over six years, but no deep minima have been recorded (the only light variability known is that with a low amplitude and a period of about 50 days [4]). Hence, so far no evidence is available that would be indicative of QY Sge to satisfy the main criterion of R CrB-type stars – sporadic dust ejections resulting in a substantial decrease of the star’s apparent brightness. The second feature different for QY Sge- and R CrB-type stars is the Doppler widths of the high-velocity emission components of the NaI doublet. These components in the spectra of R CrB-type stars are variable and so broad that they mutually overlap [20], whereas no such behavior is observed in the spectrum of QY Sge.

Third, the pattern of polarization of the emission components also differs in the two cases. It follows from spectropolarimetric observations [42] made with a resolution no higher than  $R=1000$ , the spectrum of QY Sge shows a decrease of the degree of linear polarization down to the interstellar level (emission becomes absorption as one passes from the energy distribution to the distribution of polarization degree). Such a reversal indicates that in the case of QY Sge the NaI emission forms outside the medium that polarizes the radiation of the photosphere. R CrB shows a totally different pattern. We observed this object with the spectropolarimeter of the primary focus of the 6-m telescope of SAO RAS [43] with a resolution of  $R=15000$  when the star was in a state close to minimum light. Figure 8 reproduces the figure from [43], implying that broad and narrow components of the NaI resonance doublet in the spectrum of R CrB disappeared in the wavelength dependence of the polarization degree, and polarization degree (1.5–2%) in the vicinity of the doublet is the same as in other portions of the spectrum. Note that before our observations [43] only the polarization characteristics of broad emissions were known, whereas narrow emissions were not observed because of the insufficient spectral resolution. Figure 8 leads us to conclude that the polarizing factor is located between the observer and the formation regions of the spectra of E2+BL (classification of the spectra of stars of R CrB type according to Clayton [44]). Hence QY Sge differs from R CrB also in spectropolarimetric characteristics of the sodium resonance doublet. Moreover, as we pointed out above, the  $H\beta$  line in the spectrum of QY Sge corresponds to normal hydrogen abundance (see Fig. 7), and this fact also disproves the R CrB-type classification of QY Sge.

#### 5.5. Comparison with V510 Pup

Let us now compare the spectral peculiarities of QY Sge with the spectrum of the post-AGB star V510 Pup (it is the optical component of the IR source IRAS 08005-2356), which was also found to exhibit an emission feature in NaD [45]. Despite this similarity, the spectra of QY Sge and V510 Pup differ substantially and their differences, which are evidently due to the differences between the structure and geometry of the two systems. As is evident from Figs. 4 and 5, the NaD emission in the spectrum of QY Sge is extremely strong and exceeds the continuum level by a factor of four to five. The intensity of the emission in the spectrum of V510 Pup does not exceed 1.5 continuum intensities. This difference is of no fundamental importance, because it can be explained by different degree of shielding of the radiation of the central star. Unlike QY Sge,

spectropolarimetric observations of V510 Pup do not show the decrease of polarization in the Na D lines, at least in low-resolution polarization spectra [42].

Trammel et al. [42] conclude that Balmer emissions in the spectrum of V510 Pup form in the vicinity of the star before the scattering on the dust component. The velocities measured from Na I D emissions and hydrogen lines for V510 Pup agree with each other [45], allowing us to preliminary conclude that the Na D emission also forms near the star. The same conclusion can be made for QY Sge: although the absorption profile of H $\alpha$  is almost completely flooded by the emission, spectropolarimetry does not reveal unpolarized H $\alpha$  emission. Note also that the pattern of the variation of the polarization degree over a wide wavelength region also differs for these stars. In the spectrum of V510 Pup the polarization degree decreases with increasing wavelength [42], and this fact is interpreted as the domination of scattered radiation in the blue part of the spectrum and partial transparency in the red emission of the disk (torus) that hides the star. In the spectrum of QY Sge the polarization degree increases with wavelength, suggesting higher scattering multiplicity at blue wavelengths and disk opaqueness at red wavelengths [42]. On the whole, the conclusions based on the analysis of the polarization pattern are consistent with the results of the comparison of the intensities of Na D: in the case of QY Sge we appear to observe the star only indirectly, and the contribution of high-velocity components of the shell dominates. The absence of polarization in Na I lines in the spectrum of V510 Pup can be interpreted as being due to the low contribution of emission compared to the radiation of the photosphere. This contribution is undetectable by low-resolution spectropolarimetry. Hence the formation regions of the Na D emission may have the same geometry in QY Sge and V510 Pup, but the localization of the Balmer emission near the V510 Pup star does not imply the same localization of the Na D emission.

However, one must admit that the emission feature in Na D cannot be viewed as indicative of the object belonging to a certain type of stars or to a fixed stage of evolution. Recall that a very strong and variable emission component of Na I D lines is observed in the spectra of such different stars as the unique star FG Sge [46], which has lost virtually all its atmosphere in the process of evolution, and the B[e] star CI Cam [47, 48], which is the optical component of an X-ray transient. Emission in resonance line is rather indicative of the gas-and-dust circumstellar medium with a set of physical parameters over a wide interval. However, if combined with spectropolarimetric observations, the data on the high-velocity motions in the vicinity of the star as inferred from the Na I D resonance doublet allows one to test the hypotheses concerning the geometry of the system.

## 6. Conclusions

The results of repeated spectroscopic observations (with the resolutions of  $R=15000$  and  $60000$ ) of the yellow supergiant QY Sge (the IR source IRAS 20056+1834) made with the 6-m telescope of SAO RAS lead us to conclude that the radial velocities measured from lines forming in the photosphere are variable. We revealed differential line shifts amounting to 10 km/s.

The complex emission-and-absorption profile of Na I D lines invariably contains a very wide emission component (it extends from  $-170$  to  $+120$  km/s). The wide emission is cut at its central part by an absorption feature, which, in turn, is parted into two by an overlapping (16 km/s at  $r=2.5$ ) emission peak. The positions of Na I D emission features remain unchanged and this fact indicates that they form in the regions that are external to the photosphere of the supergiant. The  $V_r$  dataset allows setting the systemic radial velocity equal to  $V_r=-21.1$  km/s, which corresponds to the position of the narrow emission component of Na I D.

Emission in the H $\alpha$  line floods the photospheric absorption almost completely.

The pattern of the variation of the profiles of emission and absorption lines and radial velocities measured from different details of the profiles is consistent with the model of a toroidal dust envelope

that hides the central source and bipolar cones filled with high-velocity gas. Both in the emission and absorption features we revealed details indicative of the spatial and temporal inhomogeneities in the dust and gaseous components of the object.

Absorption lines in the spectrum of QY Sge have a considerable width  $FWHM \approx 45$  km/s, which complicates substantially the analysis of the chemical composition. We used the method of model atmospheres to determine the following parameters: effective temperature  $T_{eff} = 6250 \pm 150$  K, surface gravity  $\log g = 2.0 \pm 0.2$ , and microturbulence velocity  $\xi_t = 4.5 \pm 0.5$  km/s. The chemical composition of the star’s atmosphere differs insignificantly from the solar composition: we find the star’s metallicity to be somewhat higher than the solar value with the mean overabundance of iron-peak elements V, Cr, Mn, Fe, Co, Ni, Cu, and Zn equal to  $[Met/H]_{\odot} = +0.20$ . We also found carbon and nitrogen to be slightly overabundant –  $[C/Fe] = +0.25$  and  $[N/Fe] = +0.27$  – with the C/N ratio close to its solar value. The  $\alpha$ -process elements Mg, Si, and Ca are slightly overabundant and their average relative abundance is equal to  $[\alpha/H]_{\odot} = +0.12$ , while sulfur is more overabundant,  $[S/\alpha] = +0.29$ . We found strong sodium overabundance,  $[Na/H]_{\odot} = +0.75$ , which appears to be due to the dredge-up of the matter processed in the NeNa-cycle. The abundances of heavy  $s$ -process elements are lower than the corresponding solar abundances.

On the whole, so far the observed properties of QY Sge do not give grounds to consider it as an R CrB- or RV Tau-type star. We point out the following especially important aspects besides the evident need for continuing the spectroscopy of QY Sge on a more regular basis:

- the S/N ratio must further be increased while maintaining the already achieved spectral resolution in order to more confidently outline the details of complex and variable profiles of absorption lines;
- it is desirable to use high-resolution spectropolarimetry, which would, in particular, help to refine the locations of the formation regions of individual components of the emission-and-absorption Na I D lines and other features;
- extremely valuable data on the geometry and kinematics of the system can be provided by (high angular resolution) spectra of sufficiently bright peripheric regions of the dust envelope, which make it possible to “come close” to the object and see its central part at different angles.

## Acknowledgments

This work was supported by the program “Observed manifestations of the evolution of the chemical composition of stars and of the Galaxy” funded by the Presidium of the Russian Academy of Sciences, the program “Extended objects in the Universe” funded by the Division of Physical Sciences of the Russian Academy of Sciences, and by the Civil Research and Development Foundation (CRDF, project RUP1-2687-NA-05). The work is supported by the Russian Foundation for Basic Research (project no. 07-02-00247). Our research made use of SIMBAD and VALD databases and ALADIN interactive sky atlas of the Strassbourgh CDS.

## References

1. P. N. Kholopov, N. N. Samus', M. S. Frolov, et al., *General Catalogue of Variable Stars*, Edition 4.1, 1998. <http://www.sai.msu.su/groups/cluster/gcvs/gcvs>.
2. T. M. Gledhill, A. Chrysostomou, J. H. Hough, and J. A. Yates. *MNRAS*, **322**, 321, 2001.
3. T. M. Gledhill, I. Bains, and J. A. Yates. *MNRAS*, **332**, L55, 2002.
4. J. W. Menzies and P. A. Whitelock. *MNRAS*, **233**, 697, 1988.
5. N. Kameswara Rao, A. Goswami, and D. L. Lambert. *MNRAS*, **334**, 129, 2002.
6. V. E. Panchuk, J. D. Najdenov, V. G. Klochkova, et al. *Bull. Spec. Astrophys. Observ.*, **44**, 127, 1998.
7. V. E. Panchuk, V. G. Klochkova, and I. D. Naidenov. Preprint *Spec. Astrophys. Observ.*, No. 135, 1999.
8. V. G. Klochkova, S. V. Ermakov, V. E. Panchuk, et al., Preprint *Spec. Astrophys. Observ.*, No. 137, 1999.
9. V. E. Panchuk, M. Y. Yushkin, and I. D. Naidenov. Preprint *Spec. Astrophys. Observ.*, No. 179, 2003.
10. V. E. Panchuk, N. E. Piskunov, V. G. Klochkova, et al. Preprint *Spec. Astrophys. Observ.*, No. 169, 2002.
11. A. A. Ivanov, V. E. Panchuk, and V. S. Shergin. Preprint *Spec. Astrophys. Observ.*, No. 155, 2001.
12. M. V. Yushkin and V. G. Klochkova. Preprint *Spec. Astrophys. Observ.*, No. 206, 2005.
13. A. K. Pierce and J. B. Breckinridge, *Contrib. Kitt Peak Obs.* No. 559, 1973.
14. J. van Blerkom and D. van Blerkom, *Astrophys. J.* **225**, 482, 1978.
15. G. Wallerstein, *Astrophys. J.* **211**, 170, 1977.
16. L. B. F. M. Waters, C. Waelkens, M. Mayor, and N. R. Trams. *A&A*, **269**, 242, 1993.
17. E. J. Bakker, F. L. A. van der Wolf, H. J. G. L. Lamers, et al., *A&A*, **306**, 924, 1996.
18. N. Kameswara Rao, B. E. Reddy, and D. L. Lambert. *MNRAS*, **355**, 855 (2004).
19. A. Goswami, N. Kameswara Rao, D. L. Lambert, and V. V. Smith. *PASP*, **109**, 270, 1997.
20. N. Kameswara Rao, D. L. Lambert, and M. D. Shetrone. *MNRAS*, **370**, 941, 2006.
21. T. Kipper and V. Klochkova, *Inform. Bul. Var. Stars* No. 4346, 1, 1996.
22. C. S. Beals, *Pub. Dom. Astrophys. Obs. Victoria* **9**, 1, 1950.
23. J. Brand and L. Blitz, *A&A*, **275**, 67, 1993.
24. V. G. Klochkova, R. Szczerba, and V. E. Panchuk. *Astron. Lett.* **26**, 439, 2000.
25. V. G. Klochkova, V. E. Panchuk, M. V. Yushkin, and A. S. Miroschnichenko. *Astron. Rep.* **48**, 288, 2004.
26. R. L. Kurucz, CD-ROM No. 23 Smithsonian Astrophysical Observatory, Cambridge, MA, 1993.
27. N. E. Piskunov, F. Kupka, and T. A. Ryabchikova. *A&ASuppl*, **112**, 525, 1995.
28. L. S. Lyubimkov, *Khimicheskij sostav zvezd: metody i rezultaty analiza*, (Odessa, Astroprint, 1995).
29. D. Shulyak, V. Tsymbal, T. Ryabchikova, et al.,
30. N. Grevesse, A. Noels, and A. J. Sauval. *ASP Conf. Ser.* **99**, 117, 1996.
31. L. I. Mashonkina, V. V. Shimanskij, N. A. Sakhbullin. *Astron. Rep.* **44**, 790, 2000.
32. H. van Winckel, C. Waelkens, L. B. F. M. Waters, B. F. M. Laurens, F. Molster, S. Udry, E. J. Bakker, *A&A*, **336**, L17, 1998.
33. A. M. Le Squeren, P. Sivagnanam, M. Dennefeld, and P. David. *A&A*, **254**, 133, 1992.
34. B. M. Lewis, J. Eder, and Y. Terzian. *AJ*, **94**, 1025, 1987.
35. T. Maas, H. van Winckel, and T. Lloyd Evans. *A&A*, **429**, 297, 2005.

**Table 1.** Log of observations of QY Sge, residual intensities “ $r$ ” and heliocentric radial velocities for different groups of lines. Uncertain values are printed in italics

Date	10.07.98	14.07.98	27-30.07.02	16.08.03	28.08.04
Spectrograph	PFES	NES	NES	NES	NES
$\Delta\lambda$ , nm	400–770	500–590	480–670	530–660	530–660
<u>FeI (15)</u>					
$r$	–	0.52	0.53	0.61	0.56
$V_r$	–9	–8	–10	–3	–13
$\Delta V_r$	–	<i>–27, +29</i>	<i>–27, +24</i>	<i>–23, +27</i>	<i>–34, +24</i>
$r_{max}$	0.90	–	0.86	0.93	0.86
$V_r$	–21	–	–14	–3	–25
<u>D2, NaI (1)</u>					
narrow emission					
$r$	3.2	5.7	4.9	5.0	5.9
$V_r$	–22	–21	–21	–21	–21
wide emission					
$r$	2.8	2.8	2.8	3.0	3.2
$V_r$	–33	<i>–31</i>	–33	–32	–33
absorption					
$r$	1.6	0.4	0.1	0.1	0.1
$V_r$	–18	<i>–17</i>	–17	–17	–18
$\Delta V_r$	–	<i>–70</i>	<i>–80</i>	<i>–75</i>	<i>–80</i>
<u>H<math>\alpha</math></u>					
absorption					
$r$	0.73	–	0.75	0.79	0.89
$V_r$	–23	–	<i>–17</i>	<i>–13</i>	–30

36. V. G. Klochkova, V. E. Panchuk, and N. S. Tavolzhanskaya. *Astron. Lett.* **28**, 49 (2002).
37. H. van Winckel, R. D. Oudmajer, and N. R. Trams, *A&A*, **312**, 553, 1996.
38. G. Wallerstein. *PASP*, **114**, 689, 2002.
39. D. Gillet, G. Burki, and A. Duguennoy. *A&A*, **237**, 159, 1990.
40. N. Kameswara Rao and D. L. Lambert. *AJ*, **105**, 1915, 1993.
41. A. Goswami, N. Kameswara Rao, and D. L. Lambert. *The Observatory*, **119**, 22, 1999.
42. S. Trammell, H. L. Dinerstein, and R. W. Goodrich. *AJ*, **108**, 984, 1994.
43. V. E. Panchuk, V. G. Kotova, N. S. Yushnkin, et al. 2001, Preprint *Spec. Astrophys. Obs. No. 159*, 2001.
44. G. C. Clayton. *PASP* 108, 225, 1996.
45. V. G. Klochkova and E. L. Chentsov. *Astron. Rep.* **48**, 301, 2004.
46. T. Kipper, M. Kipper, and V. G. Klochkova. *A&A*, **297**, L33, 1995.
47. A. S. Miroshnichenko, V. G. Klochkova, K. S. Bjorkman, and V. E. Panchuk. *A&A*, **390**, 627, 2002.
48. R. I. Hynes, J. S. Clark, E. A. Barsukova, et al. *A&A*, **392**, 991, 2002.



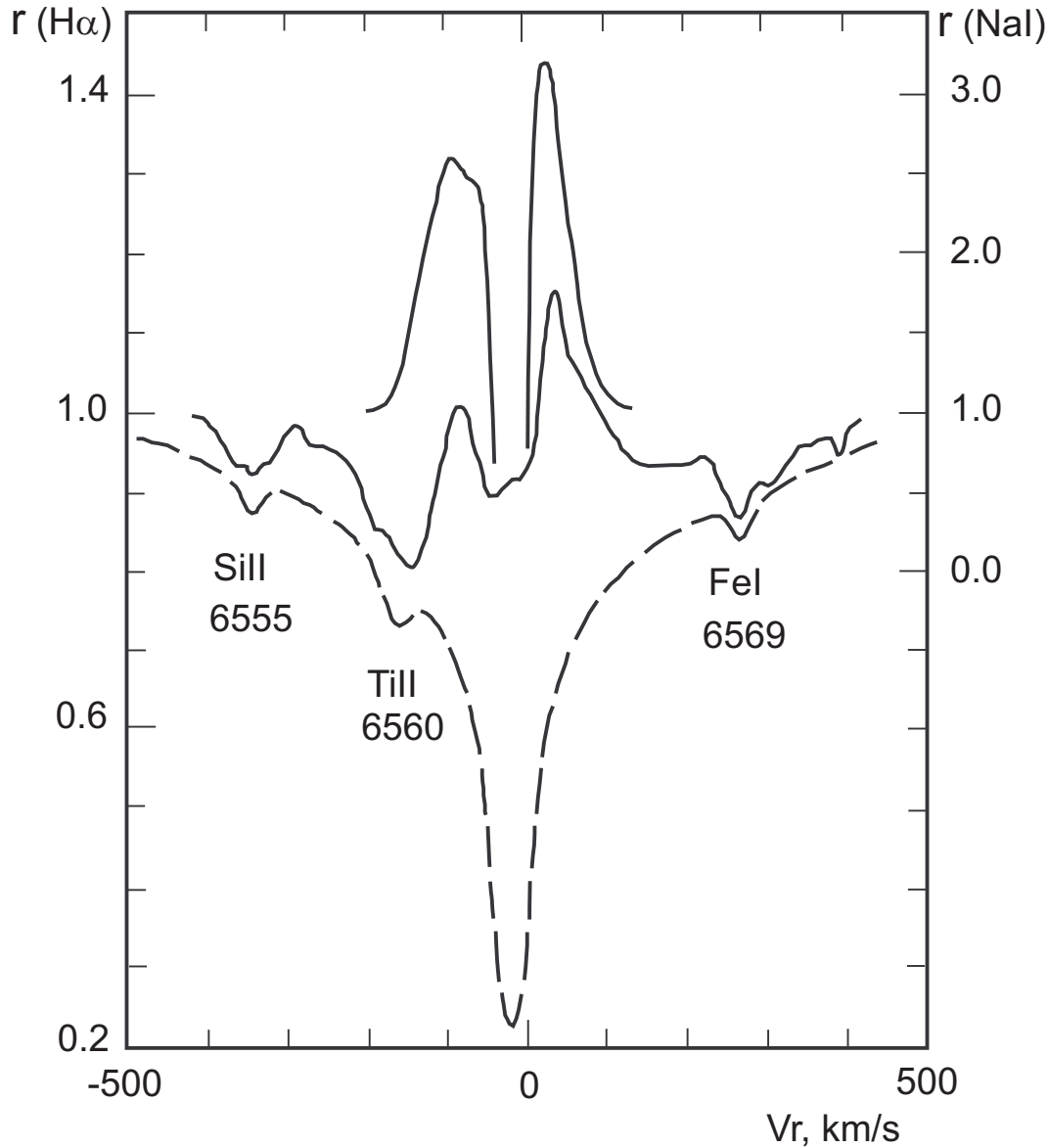


**Figure 1.** From top to bottom: NaI 5890 Å and H $\alpha$  line profiles in the spectrum of QY Sge taken on August 28, 2004 and the profile of the H $\alpha$  line in the spectrum of  $\alpha$  Per. Telluric absorptions and the central NaI emission are removed and the profiles are smoothed. The  $r$  scales for the H $\alpha$  and NaI lines are shown on the left and right, respectively.

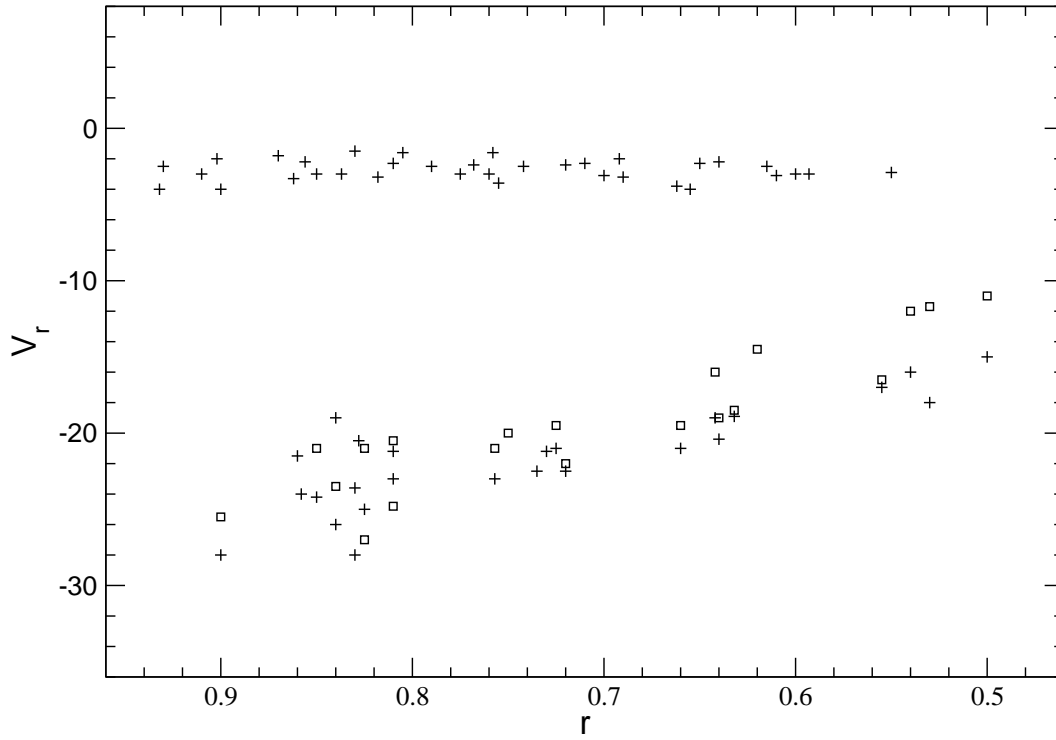


**Figure 2.** Heliocentric radial velocity as a function of the central residual line intensity in the spectra of QY Sge taken in 2003 (top) and 2004 (bottom, the crosses and squares show the  $V_r$  values inferred from the entire lines and their cores, respectively).

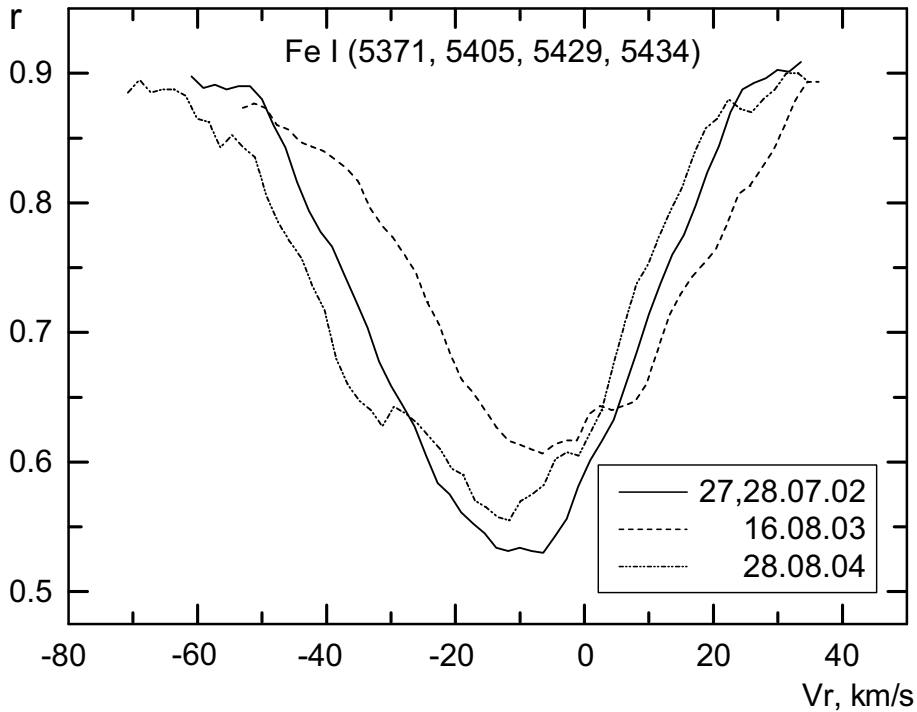


**Figure 3.** Comparison of the averaged profiles of the Fe I (15) group of lines in the spectra taken in 2002, 2003, and 2004.

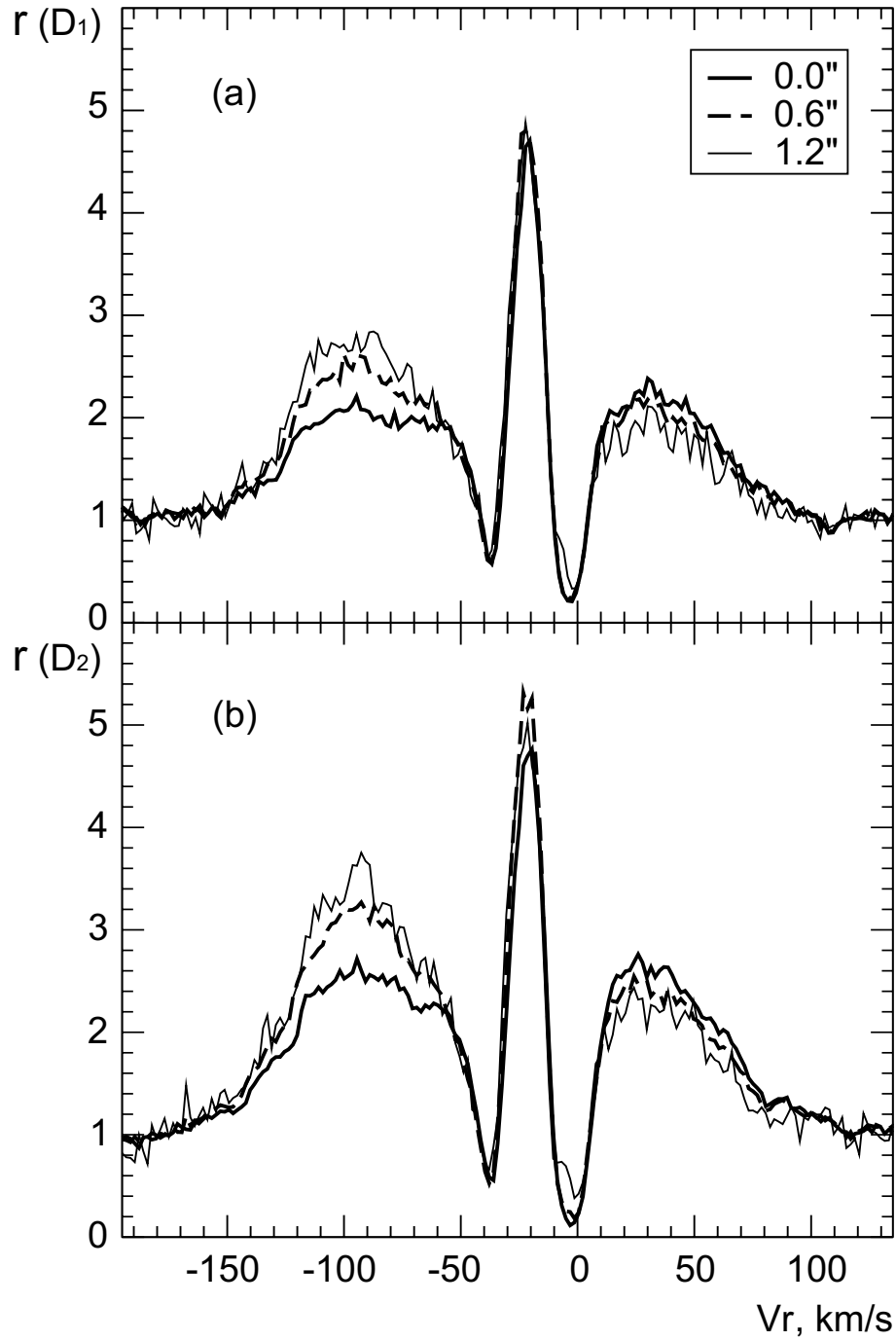


**Figure 4.** Profiles of the NaI D1 (top) and D2 (bottom) lines in the spectrum of QY Sge (observed on August 16, 2003) at different distances from the center of the star's image.

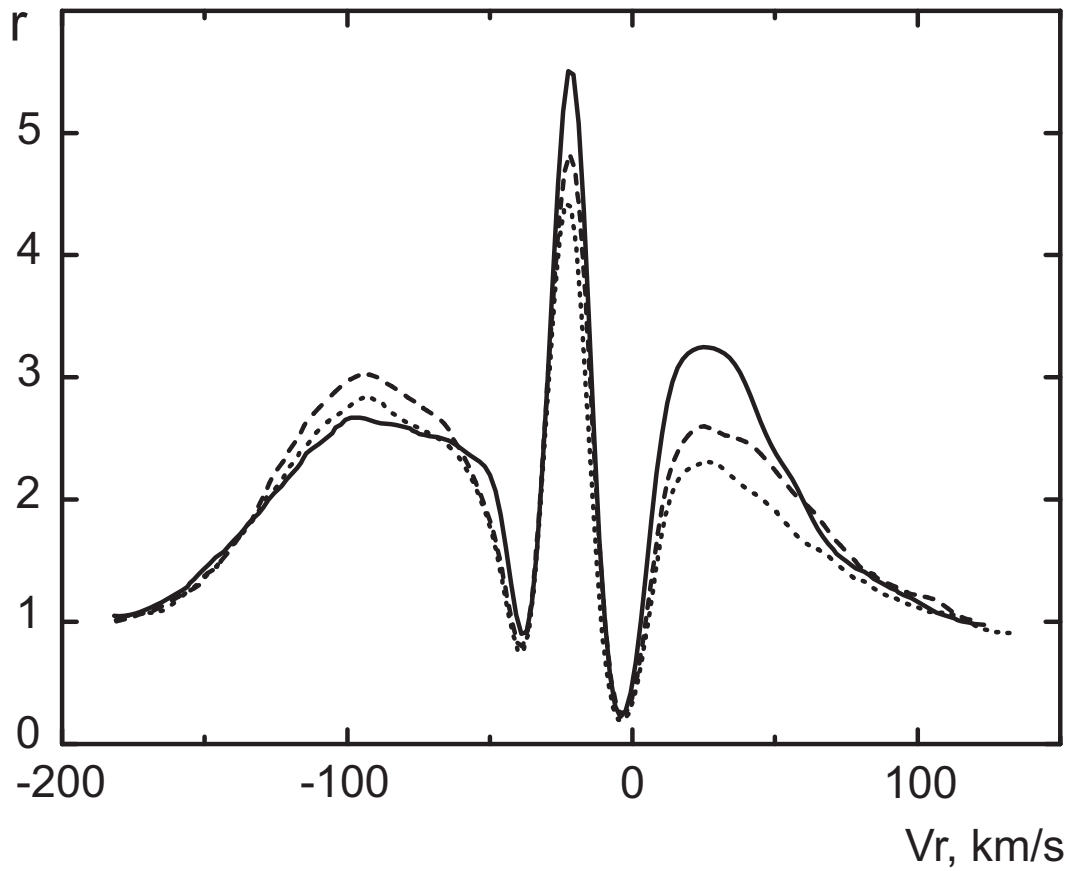


**Figure 5.** Temporal variations of the profile of the NaI D2 line in the spectrum of QY Sge. The dotted, dashed, and solid lines show the data for 2002, 2003, and 2004, respectively. Telluric absorptions are removed and the profiles are smoothed.

$$T_{\text{eff}} = 6250\text{K}, \lg g = 2.0, \xi_t = 4.5\text{km/s}$$

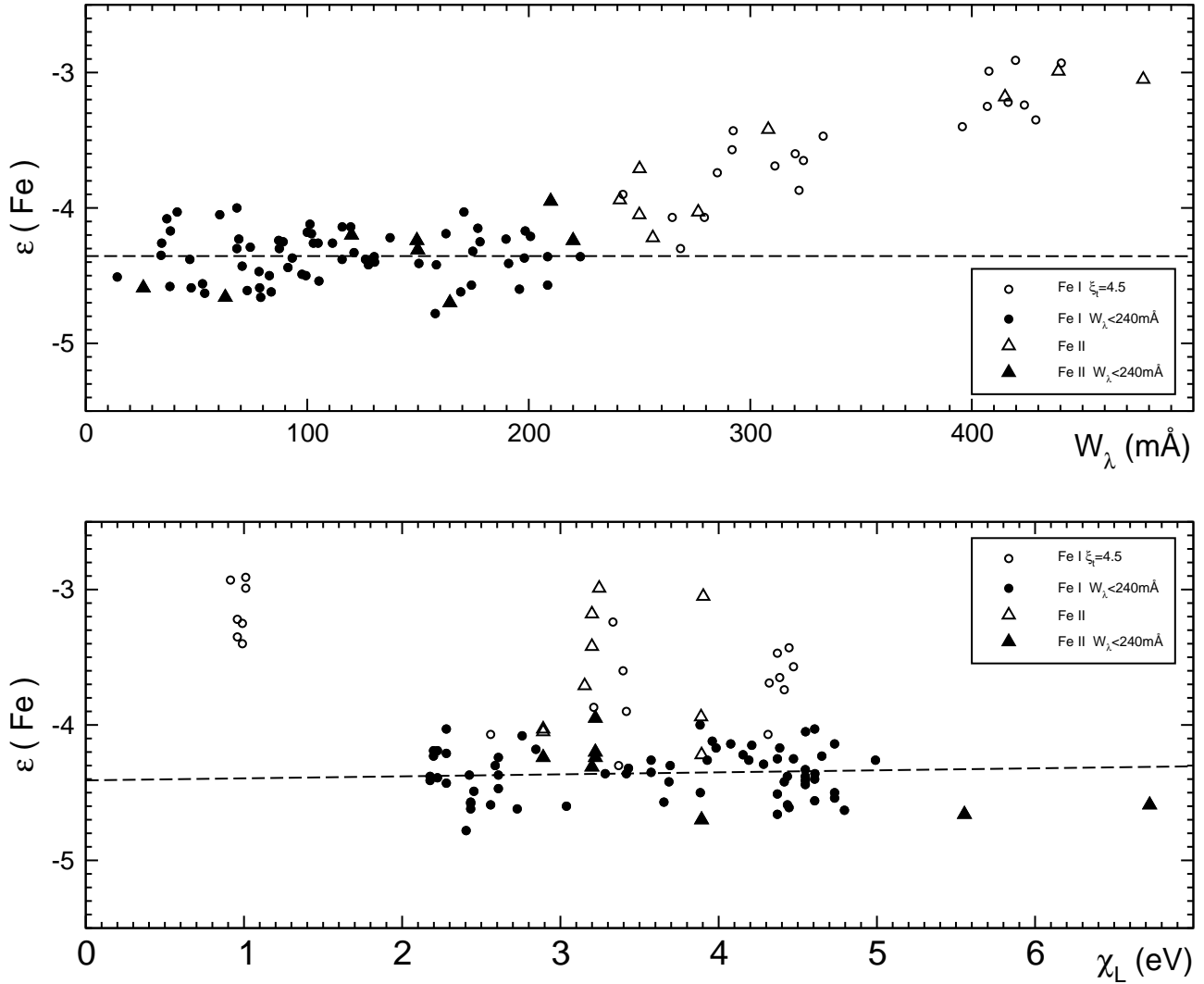


**Figure 6.** Iron abundances,  $\log \epsilon(\text{Fe})$ , determined from Fe I and Fe II lines as a function of: (a) equivalent line width  $W_\lambda$  and (b) excitation potential  $\chi_L$  of the lower level.

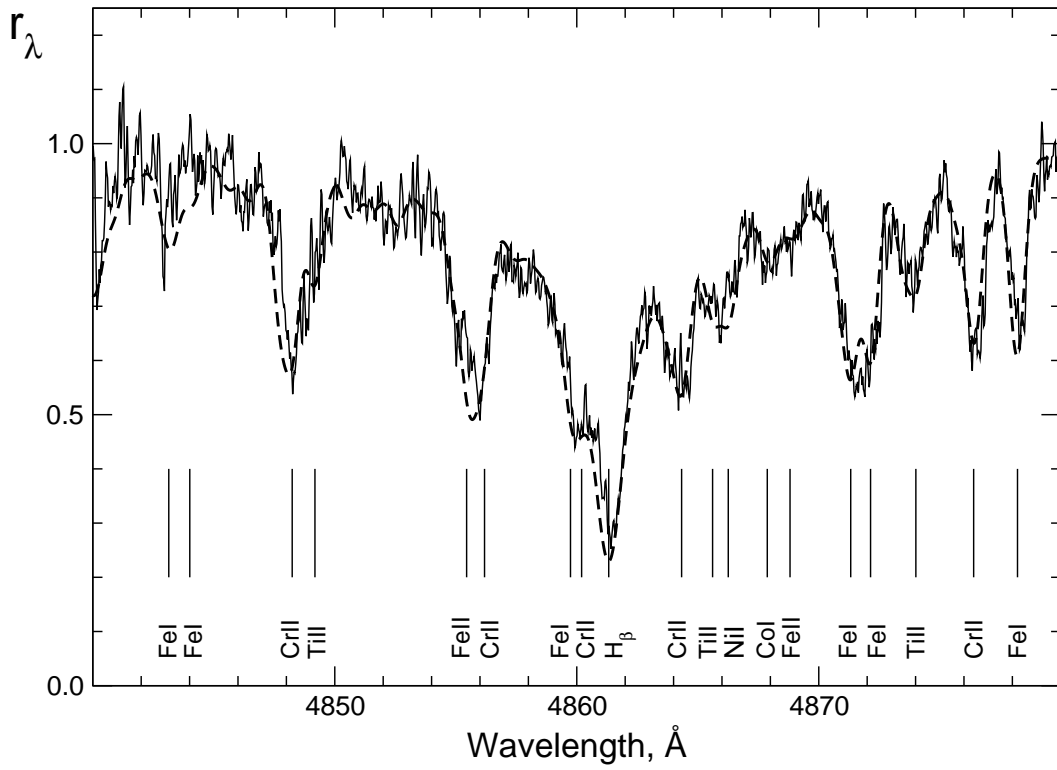


**Figure 7.** Comparison of the observed (the solid line) spectrum of QY Sge in the region of  $H_{\beta}$  line and the theoretical spectrum computed with parameters  $T_{eff} = 6250$  K,  $\log g = 2.0$ , and  $\xi_t = 4.5$  km/s and metallicity  $[Fe/H]=0$ .

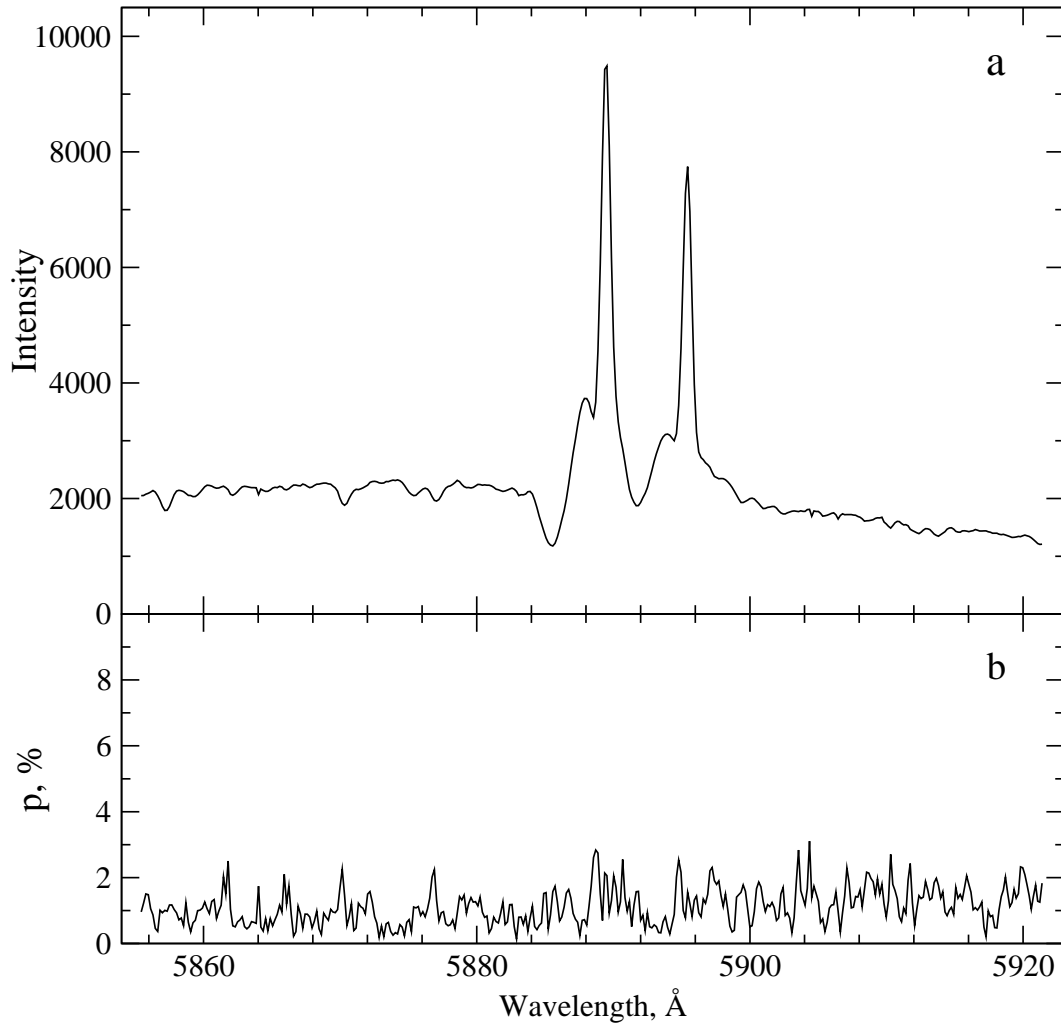


**Figure 8.** Observations of R CrB at minimum light 43: (a) the portion of the spectrum near NaID, (b) the polarization spectrum  $P, \%$  in the same wavelength region.

**Table 2.** Identification of the spectrum of QY Sge and measurements of the central residual intensity  $r$  and heliocentric radial velocity  $V_r$ , km/s, based on different spectral features. See text for explanation. Uncertain values are listed in italics

Line	$\lambda$	1998		2002		2003		2004	
		$r$	$V_r$	$r$	$V_r$	$r$	$V_r$	$r$	$V_r$
MnI(2)	4030.75	0.28	<i>-18</i>						
MnI(2)	4034.48	0.43	<i>-13</i>						
H $\delta$	4101.74	0.20	<i>-18</i>						
TiII(105)	4163.65	0.62	<i>-12</i>						
SrII(1)	4215.52	0.41	<i>-14</i>						
FeI(152)	4222.21	0.64	<i>-10</i>						
FeI(152)	4235.93	0.39	<i>-11</i>						
CrI(1)	4254.33	0.59	<i>-5</i>						
CrI(1)	4274.80	<i>0.50</i>	<i>-4</i>						
CaI(5)	4318.65	0.79	<i>-12</i>						
H $\gamma$	4340.47	0.23	<i>-12</i>						
FeI(41)	4404.75	0.38	<i>-8</i>						
FeI(350)	4476.04	0.74	<i>-13</i>						
FeI(68)	4494.57	0.58	<i>-13</i>						
FeII(38)	4508.28	0.67	<i>-9</i>						
FeII(37)	4520.22	0.63	<i>-9</i>						
BaII(1)	4554.03	0.55	<i>-4</i>						
FeII(38)	4576.33	0.70	<i>-9</i>						
CrII(44)	4588.20	0.71	<i>-11</i>						
TiII(50)	4589.95	0.75	<i>-8</i>						
FeI(39)	4602.94	0.72	<i>-11</i>						
FeII(37)	4629.33	0.70	<i>-10</i>						
FeI(820)	4643.46	0.86	<i>-9</i>						
MgI(11)	4702.99	0.70	<i>-19</i>						
FeII(43)	4731.47	0.67	<i>-11</i>						
FeI(38)	4733.59	0.77	<i>-9</i>						
FeI(554)	4736.78	0.68	<i>-10</i>						
MnI(16)	4754.04	0.77	<i>-9</i>						
FeI(821)	4768.33	0.81	<i>-10</i>						
TiII(92)	4779.98	0.79	<i>-15</i>						
MnI(16)	4783.42	0.78	<i>-7</i>						
TiII(92)	4805.09	0.75	<i>-13</i>						
H $\beta$	4861.33	0.35	<i>-9</i>	0.30	<i>-10</i>				
FeI(318)	4878.20	0.72	<i>-11</i>	0.65	<i>-14</i>				
FeI(318)	4920.50	0.63	<i>-12</i>	0.50	<i>-7</i>				
FeII(42)	4923.92	0.54	<i>-5</i>	0.39	<i>-9</i>				
1	2	3	4	5	6	7	8	9	10



Line	$\lambda$	1998		2002		2003		2004	
		r	$V_r$	r	$V_r$	r	$V_r$	r	$V_r$
Cl(13)	4932.05	0.84	-17						
BaII(1)	4934.08	0.55	-13	0.43	-9				
FeI(687)	4950.11	0.83	-12						
FeI(687)	4966.09	0.75	-17						
FeI(984)	4973.11	0.88	-13	0.80	-13				
FeI(966)	4978.60	0.83	-13						
NiI(112)	4980.18	0.83	-15	0.74	-14				
FeI(16)	5012.07	0.71	-12	0.56	-5				
FeII(42)	5018.44	0.56	-21	0.36	-12				
ScII(23)	5031.02	0.81	-14						
FeI(114)	5049.83	0.70	-16						
FeI(1)	5060.08	0.70	-14	0.65	-11				
FeI(383)	5068.76			0.70	-10				
FeI(1094)	5074.75	0.80	-9						
FeI(1)	5110.41	0.50	-9	0.42	-10				
FeI(16)	5127.36	0.69	-6	0.56	-5				
FeI(1089)	5162.27	0.75	-14						
FeI(1)	5166.28	0.5	-9	0.49	-9				
MgI(2)	5167.32	0.5	-2	0.47	-1				
FeII(42)	5169.03	0.5	-14	0.35	-9				
MgI(2)	5172.68	0.55	-10	0.50	-6				
MgI(2)	5183.61	0.52	-2	0.44	-3				
FeI(66)	5202.33	0.78	-9	0.69	-13				
FeI(383)	5232.94			0.56	-10				
FeII(49)	5234.62	0.70	-13						
FeI(1)	5247.06	0.61	-12						
FeII(49)	5254.93	0.64	-10	0.55	-10				
FeI(383)	5281.79	0.74	-12	0.72	-12	0.78	-4		
FeI(929)	5288.53	0.93	-17						
FeI(553)	5302.30					0.76	-3		
CrII(24)	5305.86	0.84	-12	0.78	-16	0.83	-3		
CrII(43)	5313.58					0.81	-2		
FeII	5316.65	0.66	-6	0.52	-9	0.55	-3	0.56	-17
FeI(553)	5324.18	0.85	-10	0.64	-13	0.69	-3	0.55	-20
FeI(37)	5341.03			0.61	-12	0.65	-5		
FeI(1062)	5353.38							0.78	-19
FeII(48)	5362.86	0.75	-16	0.59	-12	0.65	-2	0.58	-15
FeI(1146)	5367.47					0.74	-4		
FeI(15)	5371.48	0.62	-12	0.52	-8	0.60	-3	0.50	-15
FeI(15)	5397.12	0.64	-9	0.53	-10	0.65	-4		
FeI(15)	5405.77	0.64	-10	0.54	-9	0.61	-3	0.53	-12
CrII(23)	5420.93							0.72	-25
1	2	3	4	5	6	7	8	9	10

Line	$\lambda$	1998		2002		2003		2004	
		r	$V_r$	r	$V_r$	r	$V_r$	r	$V_r$
FeI(15)	5429.70	0.64	-8	0.52	-9	0.60	-3	0.54	-14
FeI(15)	5434.53	0.68	-7			0.64	-2	0.56	-17
FeI(1144)	5441.34					0.93	-3		
FeI(1163)	5445.05							0.74	-21
FeI(15)	5455.61			0.57	-9				
FeI(15)	5497.51	0.76	-12	0.68	-10	0.69	-2	0.65	-19
FeI(15)	5506.78							0.67	-17
CrII(50)	5508.62					0.82	-3		
ScII(31)	5526.82					0.74	-2		
MgI(9)	5528.40	0.72	-12	0.64	-14	0.66	-4	0.61	-14
FeI(1183)	5565.71	0.89	-11					0.82	-19
FeI(686)	5572.84	0.74	-9			0.72	-2		
FeI(686)	5586.76			0.63	-11	0.72	-2		
FeI(686)	5615.65					0.64	-3	0.62	-22
FeI(1314)	5633.95	0.89	-11	0.86	-11				
SiI(10)	5645.61	0.94	-15						
ScII(29)	5669.03	0.87	-16	0.82	-12	0.87	-1		
ScII(29)	5684.19							0.76	-22
NaI(6)	5688.21	0.76	-15	0.74	-11	0.76	-4		
FeI(1107)	5763.00			0.81	-14				
SiI(17)	5772.15	0.92	-16						
SiI(9)	5793.07					0.91	-3		
Cl(18)	5800.59	0.94	-15						
FeI(982)	5809.22	0.92	-16						
BaII(2)	5853.68	0.79	-9						
NaI(1)	5889.95	3.3	-22	4.9	-21	4.8	-21	6.0	-21
		1.7	-18	0.2	-17	0.2	-17	0.2	-18
NaI(1)	5895.92	3.0	-21	4.2	-21	4.2	-21	5.4	-21
		1.8	-18	0.3	-17	0.4	-17	0.3	-18
SiI(16)	5948.54	0.86	-11						
FeII(46)	5991.37	0.86	-16						
Cl	6014.85	0.95	-17						
NiI(27)	6016.64					0.90	-4		
FeI(1187)	6024.06					0.86	-3	0.82	-24
FeI(1018)	6027.05			0.86	-14	0.90	-1		
FeI(1259)	6056.01	0.89	-16	0.84	-13				
FeI(207)	6065.49			0.73	-13	0.83	-1		
CaI(3)	6122.22	0.81	-16	0.72	-12	0.77	-2	0.75	-21
BaII(2)	6141.72	0.70	-7	0.52	-8	0.61	-3	0.62	-14
CaI(3)	6162.17					0.76	-2		
FeI(62)	6173.34					0.91	-2		
FeI(62)	6219.29	0.85	-16			0.84	-3		
1	2	3	4	5	6	7	8	9	10

Line	$\lambda$	1998		2002		2003		2004	
		r	$V_r$	r	$V_r$	r	$V_r$	r	$V_r$
FeI(207)	6230.73	0.83	-20						
FeI(169)	6252.56					0.85	-3	0.82	-24
FeI(111)	6254.26					0.82	-3	0.81	-26
FeI(169)	6256.37					0.86	-2		
FeI(62)	6265.14	0.88	-22	0.85	-15	0.87	-1	0.83	-23
FeI(342)	6270.23							0.83	-27
FeI(169)	6344.15					0.93	-4		
SiII(2)	6347.10	0.80	-15	0.72	-11	0.72	-6	0.75	-21
FeII(40)	6369.46					0.85	-3		
SiII(2)	6371.36	0.86	-23	0.78	-13	0.80	-6		
FeI(168)	6393.61	0.87	-18	0.76	-11				
FeI(816)	6400.01							0.71	-25
FeI(816)	6411.66	0.87	-23	0.79	-12				
FeII(74)	6416.92	0.86	-17	0.75	-15	0.80	-1		
FeI(111)	6421.36	0.84	-20	0.73	-11				
FeI(62)	6430.85					0.82	-3		
FeII(40)	6432.68	0.84	-20	0.76	-11	0.79	-2	0.78	-20
CaI(18)	6439.08	0.75	-20	0.73	-13	0.77	-2	0.72	-21
CaI(19)	6449.82	0.84	-15	0.84	-12			0.82	-20
FeII(74)	6456.38	0.74	-15	0.67	-13	0.70	-3	0.67	-21
CaI(18)	6471.66	0.90	-20	0.85	-18				
H $\alpha$	6562.81	0.75	-165	0.76	-180	0.81	-95	0.75	-150
		0.73	-23	0.72	-13	0.74	-11	0.81	-26
FeI(1253)	6569.22			0.83	-12	0.87	-3		
Cl(22)	6587.61	0.87	-28						
TiII(91)	6606.95					0.93	-2		
FeI(206)	6609.12	0.92	-19						
Cl	6655.51	0.95	-14						
FeI(268)	6677.99			0.77	-12				
CaI(32)	6717.69	0.90	-17	0.88	-12				
Cl	7115.19	0.86	-26						
KI(1)	7664.87	1.6	-22						
KI(1)	7698.97	1.6	-25						
1	2	3	4	5	6	7	8	9	10

**Table 3.** Elemental abundances  $\epsilon(X)$  in the atmosphere of QY Sge. Here  $\sigma$  is the dispersion of abundances and n, the number of lines that were used in the computations. We adopt the elemental abundances  $\epsilon(X)_{\odot}$  in the solar atmosphere from [30]

X	$\epsilon(X)_{\odot}$	$\epsilon(X)$	$\sigma$	n	$[X/H]_{\odot}$	$[X/Fe]$
Cl	8.55	8.94	0.09	9	+0.39	+0.25
Ni	7.97	8.38		1	+0.41	+0.27
NaI	6.33	7.22	0.09	3	+0.89	+0.75
MgI	7.58	7.74	0.03	2	+0.14	+0.00
SiI	7.55	7.71	0.23	21	+0.16	+0.02
Si	7.21	7.62	0.09	4	+0.41	+0.27
CaI	6.36	6.43	0.12	8	+0.07	-0.07
ScII	3.17	3.16	0.22	5	-0.01	-0.15
TiI	5.02	4.84	0.10	3	-0.18	-0.32
TiII		4.60	0.09	4	-0.42	-0.56
VI	4.00	4.20	0.05	2	+0.20	+0.06
VII		4.16	0.04	3	+0.16	+0.02
CrI	5.67	5.95	0.24	5	+0.28	+0.14
CrII		6.05	0.19	9	+0.38	+0.24
MnI	5.39	5.74	0.05	3	+0.35	+0.21
FeI	7.50	7.64	0.18	66	+0.14	-
FeII		7.64	0.26	8	+0.14	-
CoI	4.92	5.10	0.06	2	+0.18	+0.04
NiI	6.25	6.49	0.19	12	+0.24	+0.10
CuI	4.21	4.38		1	+0.17	+0.03
ZnI	4.60	4.64	0.12	2	+0.04	-0.10
YII	2.24	1.56	0.03	3	-0.68	-0.82
BaII	2.13	2.60		1	+0.47	+0.33
NdII	1.50	1.46	0.28	3	-0.04	-0.18
EuII	0.51	0.91	0.04	2	+0.40	+0.26

**Table 4.** Errors of the computed abundances of various chemical elements in the atmosphere of QY Sge  $\Delta \log \epsilon(X)$ , due to the uncertainty of the determination of the atmospheric parameters of the star

X	$\Delta \log \epsilon(X)$		
	$\Delta T_{eff}$ -250 K	$\Delta \lg g$ -0.2	$\Delta \xi_t$ -0.5 km/s
Cl	+0.10	-0.15	+0.02
Ni	+0.18	-0.15	+0.03
NaI	-0.12	-0.09	+0.13
MgI	-0.13	-0.11	+0.10
SiI	-0.11	-0.09	+0.03
Si	+0.05	-0.12	+0.04
CaI	-0.16	-0.09	+0.03
ScII	-0.08	-0.14	+0.12
TiI	-0.20	-0.08	+0.01
TiII	-0.07	-0.14	+0.08
VI	-0.22	-0.08	+0.01
VII	-0.05	-0.13	+0.01
CrI	-0.20	-0.10	+0.06
CrII	+0.01	-0.15	+0.11
MnI	-0.18	-0.09	+0.08
FeI	-0.18	-0.09	+0.07
FeII	0.00	-0.14	+0.09
CoI	-0.22	-0.09	+0.01
NiI	-0.20	-0.09	+0.03
CuI	-0.25	-0.10	+0.06
ZnI	-0.19	-0.13	+0.11
YII	-0.09	-0.13	+0.02
BaII	-0.17	-0.11	+0.26
NdII	-0.14	-0.13	+0.01
EuII	-0.10	-0.11	+0.02